AGU PUBLICATIONS

Geophysical Research Letters

RESEARCH LETTER
10.1002/2016GL071757

Key Points:
- Two to three minute quasiperiodic (QP) flares are seen in approximately half of the sequences
- QP flares can brighten in phase in the two hemispheres
- The QP flares occur on closed field lines and map to the outer dayside magnetosphere

Supporting Information:
- Supporting Information S1
- Movie S1
- Movie S2
- Movie S3
- Movie S4
- Movie S5
- Movie S6
- Movie S7
- Movie S8

Correspondence to:
B. Bonfond,
b.bonfond@ulg.ac.be

Citation:
Bonfond, B., D. Grodent, S. V. Badman, J.-C. Gérard, and A. Radioti (2016), Dynamics of the flares in the active polar region of Jupiter, *Geophys. Res. Lett.*, *43*, doi:10.1002/2016GL071757.

Received 27 OCT 2016
Accepted 29 NOV 2016
Accepted article online 5 DEC 2016

Dynamics of the flares in the active polar region of Jupiter

B. Bonfond[1], D. Grodent[1], S. V. Badman[2], J.-C. Gérard[1], and A. Radioti[1]

[1]Space Sciences, Technologies and Astrophysics Research (STAR) Institute, LPAP, Université de Liège, Liège, Belgium, [2]Department of Physics, Lancaster University, Lancaster, UK

Abstract The duskside of the polar region of Jupiter's UV aurorae, called the active region, sometimes exhibits quasiperiodic (QP) flares on timescales of 2–3 min. Based on Hubble Space Telescope Far-UV time-tag images, we show for the first time that the Northern Hemisphere also displays QP flares. The area covered by these flares can reach up to 2.4×10^8 km^2 (i.e., the whole active region) but often only involves an area an order of magnitude smaller. Using a magnetic field mapping model, we deduced that these areas correspond to the dayside outer magnetosphere. In our data set, quasiperiodic features are only seen on half of the cases, and even on a given observation, a region can be quiet for one half and blinking on the other half. Consecutive observations in the two hemispheres show that the brightening can occur in phase. Combined with the size and location of the flares, this behavior suggests that the QP flares most likely take place on closed magnetic field lines.

1. Introduction

Planetary aurorae are light emissions resulting from collisions of precipitating charged particles with atmospheric constituents. Since they are guided by the magnetic planetary field, these particles, originating from the various regions of the magnetosphere, gather around the magnetic pole. The corollary is that the auroral emissions constitute a fair summary of most of the current systems and energetic events taking place within the whole magnetosphere. At Jupiter, the aurorae are usually dominated by the current system related to the transfer of momentum between the rapidly rotating planet and the dense sheet of plasma resulting directly or indirectly from Io's volcanic activity [*Hill*, 2001; *Cowley and Bunce*, 2001]. The auroral signature of this current system generally looks like a partially complete ring, called the main emission [*Ballester et al.*, 1996; *Grodent et al.*, 2008], which only accounts for about half of the total emitted power in the UV [e.g., *Nichols et al.*, 2009]. Equatorward of the main oval are diffuse, arc-shaped, or compact emissions associated with pitch angle diffusion [*Radioti et al.*, 2009] and/or hot plasma injections in the inner/middle magnetosphere [*Mauk et al.*, 2002; *Bonfond et al.*, 2012; *Dumont et al.*, 2014; *Gray et al.*, 2016]. In the same region, the electromagnetic interaction between the moons Io, Europa, and Ganymede produces auroral footprints in the form of localized spots sometimes followed by a tail (see review by *Bonfond* [2012]). The polar region, i.e., the region located poleward of the main emission, is usually divided into three morphological components: the dark region on the dawnside, essentially devoid of UV emissions; the swirl region in the center, peppered with intermittent and chaotic bursts of emission; and the active region on the duskside [*Grodent et al.*, 2003]. The latter is the main subject of the present paper and displays a complex combination of arcs, patches, and diffuse emissions. In particular, we will focus on sudden and intense brightenings called flares [*Waite et al.*, 2001]. Because of their short duration (~1–2 min), these flares are best studied with time-tag sequences from the Space Telescope Imaging Spectrograph (STIS) on board the Hubble Space Telescope (HST). However, all time-tag sequences acquired before the refurbishing of HST in 2009 were less than 5 min long, preventing any analysis of their occurrence periodicity. The first long time-tag sequences of Jupiter's aurorae took place in 2009, with three 45 min long continuous observations of the southern hemisphere. On two of them, the flares reoccurred quasiperiodically every 2–3 min [*Bonfond et al.*, 2011]. However, these emissions took place close to the planetary limb, where the positioning uncertainties are the largest. Using the magnetic mapping model from *Vogt et al.* [2011], *Bonfond et al.* [2011] concluded that the region corresponding to the flares in the equatorial plane was in the noon-dusk part of the outer magnetosphere and probably corresponded to the dayside magnetopause. They suggested that these quasiperiodic (QP) flares could be related to pulsed reconnection on the front of the magnetopause, by analogy with the Earth case [e.g., *Fuselier et al.*, 2007]. Indeed, signatures of consecutive flux transfer events were found with a time delay of ~4 min in the Pioneer and Voyager magnetic field data [*Walker and Russell*, 1985].

Table 1. List of the Imaging Observations From the GO 12883 HST Observations Campaigns

Rootname	Date[a]	Hemisphere	CML Range	QP Flare Area (km^2)	QP Flare Period (s)
oc0v01r0q	11/14/2012 16:52:55	S	96° – 102°	-	-
oc0va1r4q	11/14/2012 17:12:01	N	108° – 112°	-	-
oc0vb1raq	11/14/2012 17:28:38	S	118° – 123°	-	-
oc0v04dyq	1/25/2013 05:38:56	S	93° – 98°	-	-
oc0va4e0q	1/25/2013 05:57:52	N	104° – 110°	2.2×10^6	90
oc0vb4e2q	1/25/2013 06:16:48	S	116° – 120°	-	-
oc0v02wpq	2/14/2013 21:46:36	S	87° – 92°	-	-
oc0va2wrq	2/14/2013 22:05:32	N	98° – 104°	-	-
oc0vb2wtq	2/14/2013 22:24:28	S	110° – 114°	-	-
oc0v03jgq	2/21/2013 22:51:56	S	99° – 104°	-	-
oc0va3jiq	2/21/2013 23:10:22	N	110° – 116°	2.4×10^8	180
oc0vb3jkq	2/21/2013 23:29:18	S	122° – 126°	-	-
oc0v05r9q	3/9/2013 05:43:03	S	83° – 88°	2.6×10^7	160
oc0va5rmq	3/9/2013 06:01:59	N	94° – 100°	3.8×10^7	200
oc0vb5ruq	3/9/2013 06:20:55	S	106° – 110°	2.0×10^7	140
oc0v07o9q	12/21/2013 07:14:22	S	108° – 112°	-	-
oc0va7obq	12/21/2013 07:31:18	N	118° – 133°	3.9×10^7	150
oc0v06xhq	1/24/2014 15:13:24	S	120° – 124°	-	-
oc0va6xjq	1/24/2014 15:30:20	N	130° – 145°	-	-

[a]Dates are formatted as month/day/year.

Given the limited amount of long time-tag sequences at the time and their unfavorable observing geometry, many questions remained unanswered. In particular, it was not known whether the QP flares are always present and, if not, what is their occurrence rate. Considering the proximity of the studied flares to the limb, large uncertainties still existed concerning their exact location and their extent. Furthermore, their propagation speed is also intriguing, as it can hardly correspond to any actual propagation speed in the magnetospheric equatorial plane.

2. Auroral Image Sequences

The present study is based on two HST observation campaigns which took place in 2013 and 2014. These two campaigns took advantage of the time-tag mode of the STIS instrument to produce long image sequences. The first one (GO 12883) consisted of views of the northern (N) and southern (S) aurora, including one or two transitions between hemispheres during seven 45 min long HST observations. The first five followed a S-N-S pattern with exposure times from 391 to 530 s in each hemisphere. The last two followed a S-N pattern, focusing for 410 s on the southern aurorae and then 1456 s on the northern one. The second campaign (GO 13035) consisted of 14 orbits dedicated to the northern aurora only [*Badman et al.*, 2016]. Each orbit consisted of two imaging observations (700 s and 736 s long, respectively) interspersed by a 200 s long spectral observation. All the imaging time-tag sequences used in the present study were acquired with the strontium fluoride filter, which excludes the Lyman-α line and thus reduces both the count rate on the detector and the contamination by geocoronal emissions. The time-tag event sequences have been sliced into 10 s frames processed with the standard HST "CALSTIS" calibration pipeline from the Space Telescope Science Institute for dark count, flat-field, and geometrical corrections. The conversion from counts to either kilo-Rayleighs (kR) or watts is based on the conversion coefficients from *Gustin et al.* [2012], assuming a typical color ratio of 2.5. The localization of the planetary center was performed through the limb-fitting method described in *Bonfond et al.* [2009]. However, the center location sometimes had to be manually corrected because of the lack of limb points on one side of the aurora on several images. The planetary disk subtraction used the extrapolation method from *Bonfond et al.* [2011].

Table 2. List of the Imaging Observations From the GO 13035 HST Observations Campaigns

Rootname	Date[a]	Hemisphere	CML Range	QP Flare Area (km^2)	QP Flare Period (s)
oc1z01loq	1/1/2014 03:02:53	N	173° – 180°	-	-
oc1z01luq	1/1/2014 03:32:45	N	191° – 199°	-	-
oc1z02twq	1/2/2014 09:19:53	N	192° – 199°	-	-
oc1z02u2q	1/2/2014 09:49:45	N	210° – 217°	-	-
oc1z03y3q	1/3/2014 04:27:26	N	166° – 173°	4.8×10^6	80
oc1z03ybq	1/3/2014 04:57:18	N	184° – 191°	7.7×10^6	130
oc1z04b4q	1/4/2014 01:10:40	N	197° – 204°	-	-
oc1z04bbq	1/4/2014 01:40:22	N	215° – 222°	-	-
oc1z05haq	1/5/2014 05:52:00	N	158° – 165°	-	-
oc1z05hgq	1/5/2014 06:21:52	N	176° – 184°	1.2×10^7	90
oc1z06ayq	1/6/2014 02:35:18	N	190° – 197°	2.5×10^7	100
oc1z06b4q	1/6/2014 03:05:10	N	208° – 215°	-	-
oc1z07jnq	1/7/2014 07:16:40	N	151° – 158°	-	-
oc1z07jtq	1/7/2014 07:46:32	N	169° – 176°	1.1×10^8	120
oc1z09f4q	1/10/2014 03:48:48	N	117° – 124°	3.7×10^7	210
oc1z09faq	1/10/2014 04:18:40	N	135° – 142°	4.7×10^7	150
oc1z10hrq	1/11/2014 00:31:58	N	149° – 156°	-	-
oc1z10hxq	1/11/2014 01:01:50	N	167° – 174°	-	-
oc1z11lfq	1/11/2014 19:39:29	N	122° – 129°	5.2×10^7	120
oc1z11llq	1/11/2014 20:09:21	N	140° – 148°	3.5×10^7	140
oc1z13b4q	1/13/2014 01:56:15	N	141° – 148°	-	-
oc1z13baq	1/13/2014 02:26:07	N	159° – 166°	-	-
oc1z14e4q	1/13/2014 21:03:44	N	115° – 122°	-	-
oc1z14eaq	1/13/2014 21:33:36	N	133° – 140°	-	-
oc1z08edq	1/13/2014 22:39:21	N	172° – 180°	-	-
oc1z08ejq	1/13/2014 23:09:13	N	191° – 198°	-	-
oc1z12mjq	1/16/2014 00:03:33	N	165° – 172°	-	-
oc1z12mqq	1/16/2014 00:33:25	N	183° – 190°	-	-

[a]Dates are formatted as month/day/year.

3. Analysis of the QP Flares

3.1. Occurrence Rates and Duration

While sudden brightness enhancements in the active region are identified in every sequence, only approximately half of them (10 over 21) displays an unambiguous quasiperiodic pattern (see Tables 1 and 2). One example can be found in Figure 1a, where a faint arc of emission located just poleward of another arc connected to the main emission on the noon side brightens and dims every ~3 min (see also Movies S1 and S2 in the supporting information). It is noteworthy that one of the oscillations appears to be missing at the end of the sequence (around 2350 s).

Moreover, on one of these sequences, the quasiperiodic pattern is absent from the first 700 s, only to appear in the second segment of the sequence (see Figure 1b and Movies S3 and S4). In this 45 min long sequence, a V-shaped feature (highlighted with a green circle) slowly migrates from around 159° of S_{III} longitude and 66° of latitude at the beginning of the sequence to around 163° of S_{III} longitude and 62° of latitude at the end. Its emitted power first increases sharply over 100 s before it steadily decreases during the next 300 s before modestly increasing again for ~500 s. Then, for 1000 s, the imaging observations are interrupted by a spectral observation and its related overhead. When the imaging observations start back, the feature begins to blink every 120 s with a progressively decreasing peak amplitude.

In the GO-12883 campaign, five observations have been carried in a S-N-S sequence. During such a sequence, the CML range is a trade-off allowing a good view of the Ganymede footprint in each hemisphere. This range is

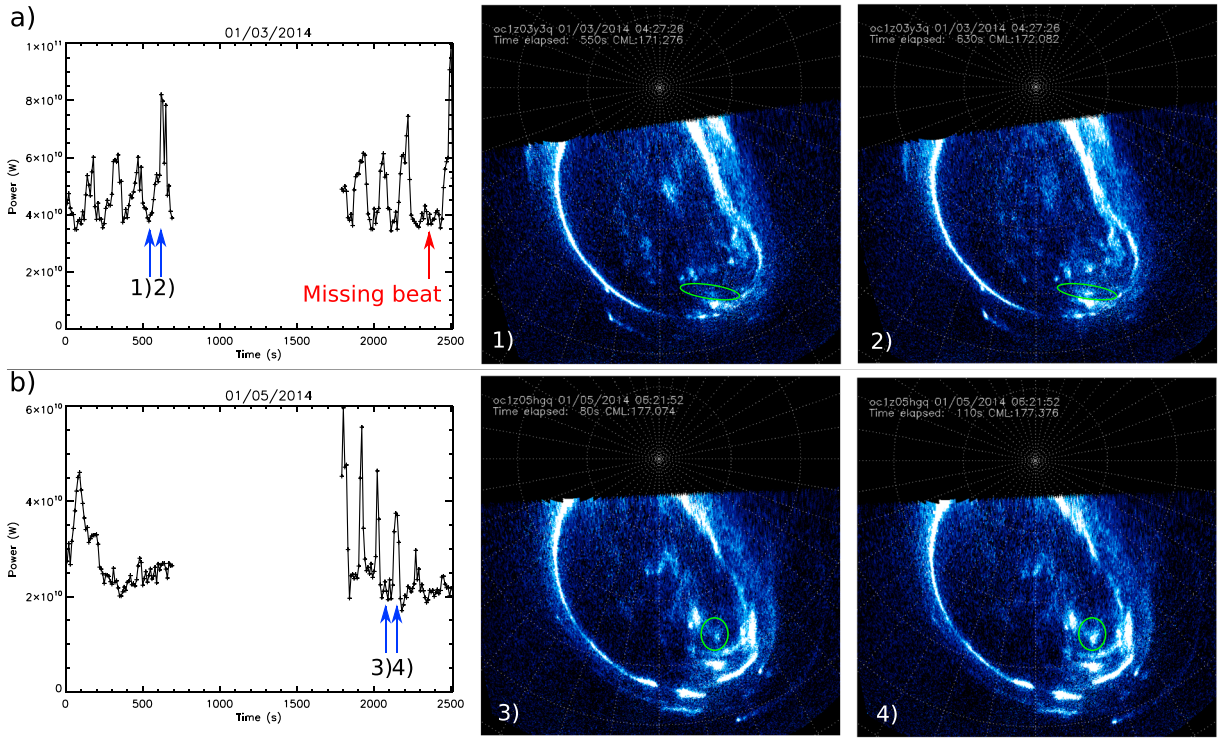

Figure 1. (a, b) The evolution of the emitted power in the area outlined in the polar projections displayed in the right panels. Brightness (1, 3) minima and (2, 4) maxima. The top panels correspond to the observations carried out on 3 January 2014. It can be seen that the QP behavior is present all along the sequence, but one beat seems missing at 2350 s (red arrow). The bottom panels correspond to the observations carried out on 5 January 2014. In this second example, it can be seen that the QP behavior only takes place in the second half of the sequence.

thus not optimum for viewing of the polar region of the two hemispheres, and only a limited part of it appears on the images. As a consequence, the counterpart of a flare in the north is often hidden behind the limb in the south, preventing any meaningful comparison. Nevertheless, on 9 March 2013, some QP activity can be seen on both hemispheres. Figure 2 and Movies S5–S7 show a polar projection of the three consecutive time-tag sequences and the evolution of the flare's integrated power on each of them. Both the baseline and the amplitude of the variations differ, but it is not clear whether these differences between the hemispheres are real or due to the difference of the area in sight of HST at the time. A sine curve with a 140 s period is overplotted, demonstrating that the signals from both hemispheres are remarkably in phase, which is indicative of a connection between the hemispheres.

3.2. Location and Propagation

The region showing a quasiperiodic behavior is first selected manually on the polar projections, based on a visual inspection of the animated sequences. The image pixels corresponding to this region are then identified on each individual frame in order to build the time series of the power as shown on Figure 1. In order to determine the area impacted by the flare in a less arbitrary way, System III fixed 360 by 180 pixel cylindrical projections of each 10 s frame are built and a time series is derived for each 1° × 1° pixel. The correlation coefficient between this series and the manually selected time series is then computed for each pixel. Only the points for which the correlation coefficient is higher than 0.7 are considered part of the flare. It is the surface covered by these points that are reported in Tables 1 and 2.

In Figure 1, the regions showing a QP behavior is limited to areas 1.8×10^7 km^2 and 1.7×10^7 km^2 wide, respectively. However, on the sequence acquired on 21 February 2013, the surface covered by three consecutive flares is much larger, as the brightness over the whole $\sim2.4\times10^8$ km^2 large active region increases simultaneously (see Figure 3 and Movie S8). No significant delay can be seen in the time series of distant points within the flare. The flaring feature appears to be limited by the main emission on the duskside and by a sharp boundary on the side closest to the magnetic pole. Magnetic field mapping models from *Vogt et al.* [2015] indicate that this area connects to an enormous sector of the magnetosphere, ranging from ~30 Jovian radii (R_J) to ~90 R_J in radial distances and from 12 to 18 in local time. Moreover, the location of the sharp brightness

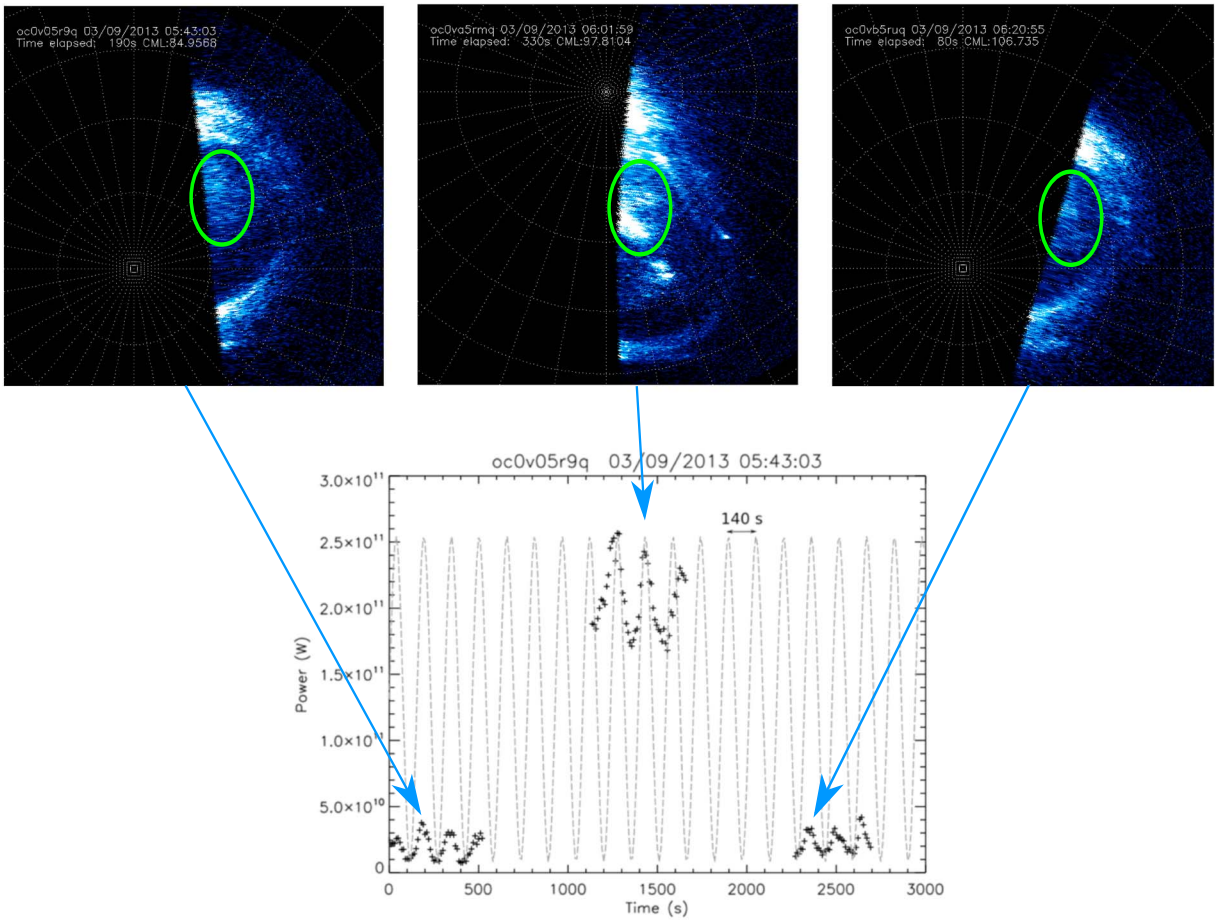

Figure 2. (top row) the polar projection of the three consecutive time-tag sequences acquired on 9 March 2013. HST first observed the (left) southern hemisphere, then the (middle) northern one, then the (right) southern one again. (bottom) The time series of the emitted power in the active region. The periodicity of the emissions is obvious, with a reoccurrence time of 140 s. Moreover, this plot shows that both hemispheres brighten in phase, as highlighted by the dashed sine function superposed to the data.

boundary inside the polar region appears to correspond approximately to the open-close field line boundary in the models. It should however be noted that such models are increasingly inaccurate as one moves toward the pole and the uncertainty can be as large as 30 R_J and 1 h in local time [*Vogt et al.*, 2015].

Figure 4 shows how all the points identified with the QP flares map into the equatorial plane using the model of *Vogt et al.* [2015] with VIPAL [*Hess et al.*, 2011] as the internal field model. Most of these points correspond to closed field lines and essentially map to the dayside outer magnetosphere. Their local time ranges from ~6 to ~18, and their radial distance ranges from ~30 to 100 R_J.

4. Discussion and Conclusions

The first detection of quasiperiodic flares on timescales of 2–3 min only concerned a very limited set of observations [*Bonfond et al.*, 2011], and it was not clear if the conclusions derived from them could be generalized. The quasiperiodic flares may also have been observed in Far-UV spectral observations. For example, two consecutive brightness enhancements 150 s apart have been observed on 4 July 1997 in the polar region [*Gérard et al.*, 2003]. The color ratio was relatively low (~2.2) and remained constant while the brightness varied. In the spectral scan of the aurora from 8 January 2014 [*Gérard et al.*, 2014], they would appear as parallel bands aligned with the slit as it sweeps through the polar regions. Because they are exactly parallel to the slit, the stripe pattern is most likely due to temporal variations rather than spatial variations. Again, the color ratio in this region was relatively low (~2), indicating that the stripes are caused by lower energy electrons compared to those creating the neighboring bright feature with a color ratio >10.

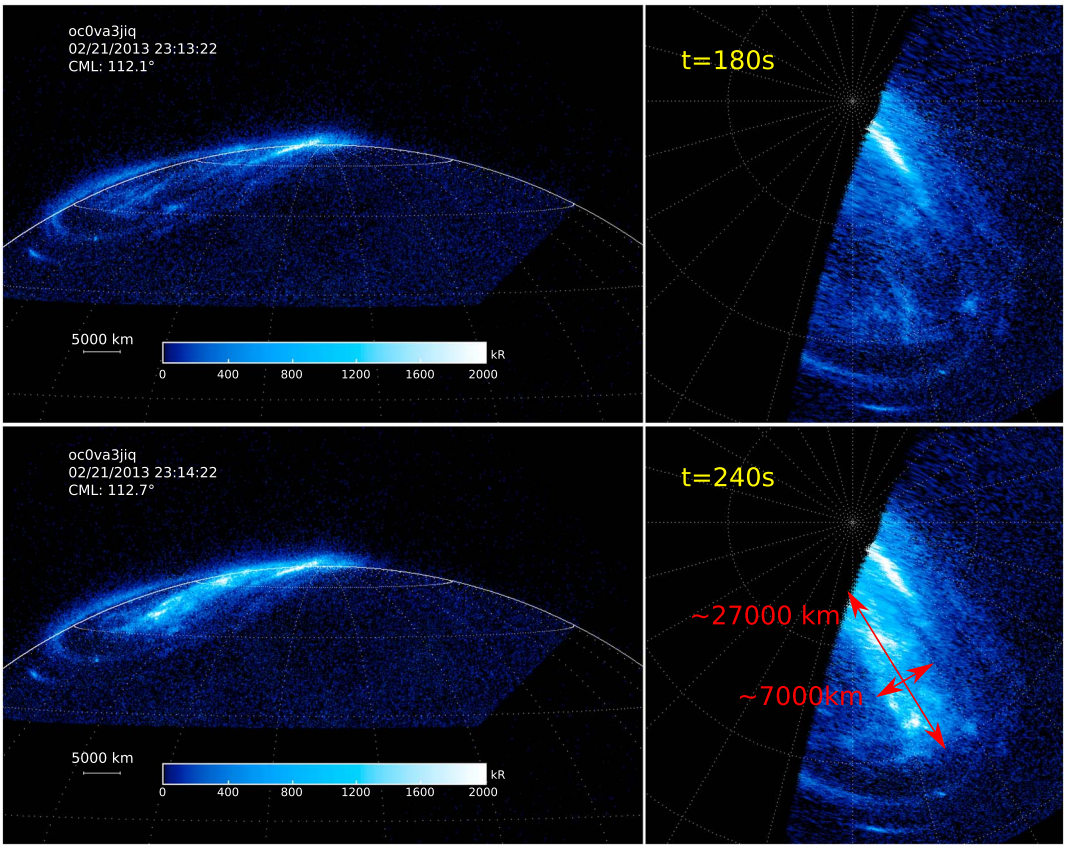

Figure 3. Image and polar projections of the northern aurorae from a time-tag sequence acquired on 21 February 2013. The 30 s exposures starting at (top row) 180 s and (bottom row) 240 s after the start of the observation, respectively. The area involved in the flare is roughly 27,000 km × 7000 km.

The present study is examining a much larger and better suited data set and allows us to clarify the occurrence rate and the location of these flares. A quasiperiodic behavior is identified in approximately half of the time-tag sequences acquired in 2013 and 2014. Moreover, QP flares are sometimes seen during a limited segment of the observation sequence. Additionally, one beat can occasionally be missing in a sequence of bursts.

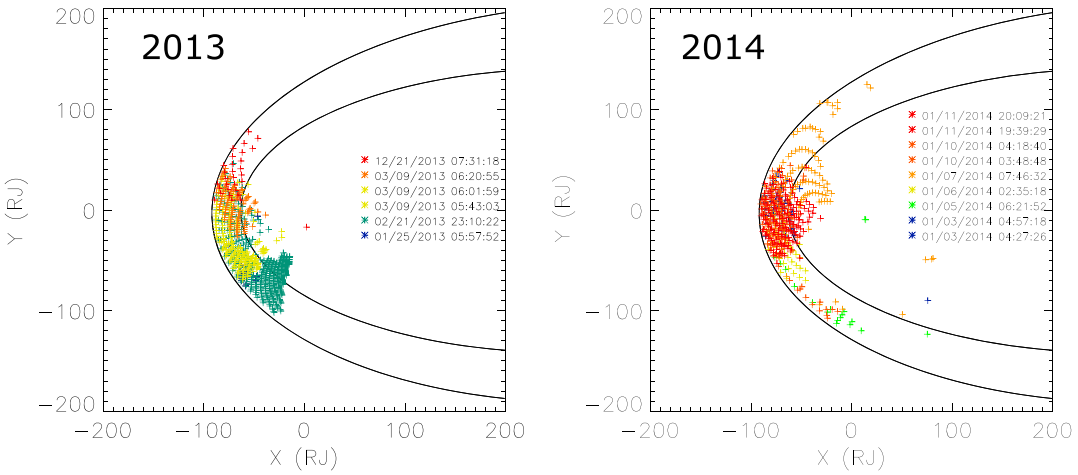

Figure 4. Mapping of the QP flares in the equatorial plane using the model of *Vogt et al.* [2015] in its VIPAL version. Each color corresponds to a particular day. The solid lines represent the expanded and compressed typical magnetopause distances according to *Joy et al.* [2002]. (left) Observations from 2013 (program GO 12883) and (right) observations from 2014 (program GO 13035). It can be seen that, whatever the day, the QP flares map to the outer dayside magnetosphere.

The extent of the auroral features giving rise to the QP behavior also widely varies from $\sim 10^7$ km^2 only to the whole active region ($\sim 2.4 \times 10^8$ km^2). The mapping of these flaring regions indicates that they take place on closed field lines encompassing several tens of R_J in the equatorial plane. This conclusion is strengthened by the observations of periodic flares occurring in phase in the two hemispheres, which is a strong indication that the flares in the two hemispheres are connected. Magnetopause auroral signatures at another giant planet, Saturn, has shown that hemispheric symmetry is broken on newly opened flux tubes [*Meredith et al.*, 2013]. Additionally, multiple brightenings in the dayside aurora of Saturn, on timescales of 1 h, longer than shown here at Jupiter, are suggested to be signatures of dayside magnetopause reconnection [*Radioti et al.*, 2013]. The authors showed that the configuration according to which the auroral signatures were proposed to be on newly opened field lines required north-south auroral asymmetries.

While the symmetry observed at Jupiter does not totally rule out the tentative explanation related to pulsed reconnection on a site exactly equidistant of both poles, the enormous size (both in longitude and in latitude) of the largest flares makes it unlikely that the extent of these flares could be a direct image of the extent of the source region in the equatorial plane. There is no delay between the brightness maxima at various points of the flares in the sequence from 21 February 2013 (Figure 3). A synchronized behavior on such large areas would indeed require propagation speeds close to or even larger than the speed of light. As a consequence, while the root cause for the QP flares may still lie in the equatorial plane, their extent appears to be controlled by propagation mechanisms located much closer to the planet (i.e., in the lobes or in the ionosphere). For example, the timescale similarity with the brightness fluctuation of the satellite footprints [*Bonfond et al.*, 2007, 2013; *Grodent et al.*, 2009] could result from a characteristic frequency from the electron acceleration region. Finally, it should be noted that the solar wind was relatively quiet during the whole GO 13035 campaign [*Kimura et al.*, 2015], and yet QP flares are seen on half of these observations. As a consequence, a high solar dynamic pressure is not a necessary condition for QP flares to happen.

While most previous studies focused on periodicities from 15 to 45 min [e.g., *MacDowall et al.*, 1993; *McKibben et al.*, 1993; *Gladstone et al.*, 2002; *Pryor et al.*, 2005], periodicities on the order of a few minutes have also been observed in other data sets throughout the Jovian magnetosphere. For example, Figure 1 of *Hospodarsky et al.* [2004] shows a series of consecutive arcs ~2 min apart in radio spectrograms between 15 and 40 kHz acquired by Cassini's Radio and Plasma Wave Science instrument during the Jupiter flyby. Another example of similar periodicities in radio measurements can be found in the periodicity analysis of the emissions observed by the Plasma Waves Subsystem on board Galileo. On Figure 5 of *Kimura et al.* [2011], the periodogram shows a notable peak between 3 and 4 min. In the particle measurements, *McKibben et al.* [1993] reported bursts of high-energy electrons (>~16 MeV) with a 144 s period when Ulysses was on its outbound leg at high southern latitudes on closed field lines in the outer duskside magnetosphere. The field lines crossed by Ulysses thus mapped to the active region, where the QP flares are observed. However, such high-energy electrons would not be compatible with the color ratios discussed above. Coordinated observations between Juno's complete suite of in situ and remote sensing instruments [*Bagenal et al.*, 2014] and Far-UV HST auroral observations will most likely provide the first simultaneous set of observation of the phenomena related (or even giving rise) to these short-timescale quasiperiodic brightness enhancements in the Jovian aurorae.

Acknowledgments
B.B. was funded by the Fund for Scientific Research (F.R.S-FNRS). B.B., J.-C.G. and D.G. were supported by the PRODEX program managed by ESA in collaboration with the Belgian Federal Science Policy Office. S.V.B. was supported by an STFC Ernest Rutherford Fellowship (ST/M005534/1). This research is based on publicly available observations acquired with the NASA/ESA Hubble Space Telescope (program IDs 12883, 13035) and obtained from the Space Telescope Science Institute (https://archive.stsci.edu/hst/search.php) which is operated by AURA Inc. The authors acknowledge the support of ISSI, as this study was discussed within ISSI International Teams 357 and 388.

References

Badman, S. V., et al. (2016), Weakening of Jupiter's main auroral emission during January 2014, *Geophys. Res. Lett.*, *43*, 988–997, doi:10.1002/2015GL067366.

Bagenal, F., et al. (2014), Magnetospheric science objectives of the Juno mission, *Space Sci. Rev.*, doi:10.1007/s11214-014-0036-8.

Ballester, G. E., et al. (1996), Time-Resolved Observations of Jupiter's Far-Ultraviolet Aurora, *Science*, *274*, 409–413, doi:10.1126/science.274.5286.409.

Bonfond, B. (2012), When Moons Create Aurora: The Satellite Footprints on Giant Planets, in *Auroral Phenomenology and Magnetospheric Processes: Earth And Other Planets, Geophys. Monogr. Ser.*, vol. 197, pp. 133–140, AGU, Washington, D. C., doi:10.1029/2011GM001169.

Bonfond, B., J.-C. Gérard, D. Grodent, and J. Saur (2007), Ultraviolet Io footprint short timescale dynamics, *Geophys. Res. Lett.*, *34*, L06201, doi:10.1029/2006GL028765.

Bonfond, B., D. Grodent, J.-C. Gérard, A. Radioti, V. Dols, P. A. Delamere, and J. T. Clarke (2009), The Io UV footprint: Location, inter-spot distances and tail vertical extent, *J. Geophys. Res.*, *114*, A07224, doi:10.1029/2009JA014312.

Bonfond, B., M. F. Vogt, J.-C. Gérard, D. Grodent, A. Radioti, and V. Coumans (2011), Quasi-periodic polar flares at Jupiter: A signature of pulsed dayside reconnections?, *Geophys. Res. Lett.*, *380*, L02104, doi:10.1029/2010GL045981.

Bonfond, B., D. Grodent, J.-C. Gérard, T. Stallard, J. T. Clarke, M. Yoneda, A. Radioti, and J. Gustin (2012), Auroral evidence of Io's control over the magnetosphere of Jupiter, *Geophys. Res. Lett.*, *39*, L01105, doi:10.1029/2011GL050253.

Bonfond, B., S. Hess, J.-C. Gérard, D. Grodent, A. Radioti, V. Chantry, J. Saur, S. Jacobsen, and J. T. Clarke (2013), Evolution of the Io footprint brightness I: Far-UV observations, *Planet. Space Sci.*, *88*, 64–75, doi:10.1016/j.pss.2013.05.023.

Cowley, S. W. H., and E. J. Bunce (2001), Origin of the main auroral oval in Jupiter's coupled magnetosphere-ionosphere system, *Planet. Space Sci.*, *49*, 1067–1088, doi:10.1016/S0032-0633(00)00167-7.
Dumont, M., D. Grodent, A. Radioti, B. Bonfond, and J.-C. Gérard (2014), Jupiter's equatorward auroral features: Possible signatures of magnetospheric injections, *J. Geophys. Res. Space Physics*, *119*, 10,068–10,077, doi:10.1002/2014JA020527.
Fuselier, S. A., S. M. Petrinec, K. J. Trattner, M. Fujimoto, and H. Hasegawa (2007), Simultaneous observations of fluctuating cusp aurora and low-latitude magnetopause reconnection, *J. Geophys. Res.*, *112*, A11207, doi:10.1029/2007JA012252.
Gérard, J.-C., J. Gustin, D. Grodent, J. T. Clarke, and A. Grard (2003), Spectral observations of transient features in the FUV Jovian polar aurora, *J. Geophys. Res.*, *108*, 1319, doi:10.1029/2003JA009901.
Gérard, J.-C., B. Bonfond, D. Grodent, A. Radioti, J. T. Clarke, G. R. Gladstone, J. H. Waite, D. Bisikalo, and V. I. Shematovich (2014), Mapping the electron energy in Jupiter's aurora: Hubble spectral observations, *J. Geophys. Res. Space Physics*, *119*, 9072–9088, doi:10.1002/2014JA020514.
Gladstone, G. R., et al. (2002), A pulsating auroral X-ray hot spot on Jupiter, *Nature*, *415*, 1000–1003.
Gray, R. L., S. V. Badman, B. Bonfond, T. Kimura, H. Misawa, J. D. Nichols, M. F. Vogt, and L. C. Ray (2016), Auroral evidence of radial transport at Jupiter during January 2014, *J. Geophys. Res. Space Physics*, *121*, 9972–9984, doi:10.1002/2016JA023007.
Grodent, D., J. T. Clarke, J. H. Waite, S. W. H. Cowley, J.-C. Gérard, and J. Kim (2003), Jupiter's polar auroral emissions, *J. Geophys. Res.*, *108*, 1366, doi:10.1029/2003JA010017.
Grodent, D., J.-C. Gérard, A. Radioti, B. Bonfond, and A. Saglam (2008), Jupiter's changing auroral location, *J. Geophys. Res.*, *113*, A01206, doi:10.1029/2007JA012601.
Grodent, D., B. Bonfond, A. Radioti, J.-C. Gérard, X. Jia, J. D. Nichols, and J. T. Clarke (2009), Auroral footprint of Ganymede, *J. Geophys. Res.*, *114*, A07212, doi:10.1029/2009JA014289.
Gustin, J., B. Bonfond, D. Grodent, and J. C. Gérard (2012), Conversion from hst acs and stis auroral counts into brightness, precipitated power and radiated power for h2 giant planets J, *J. Geophys. Res.*, *117*, A07316, doi:10.1029/2012JA017607.
Hess, S. L. G., B. Bonfond, P. Zarka, and D. Grodent (2011), Model of the Jovian magnetic field topology constrained by the Io auroral emissions, *J. Geophys. Res.*, *116*, A05217, doi:10.1029/2010JA016262.
Hill, T. W. (2001), The Jovian auroral oval, *J. Geophys. Res.*, *106*, 8101–8108, doi:10.1029/2000JA000302.
Hospodarsky, G. B., W. S. Kurth, B. Cecconi, D. A. Gurnett, M. L. Kaiser, M. D. Desch, and P. Zarka (2004), Simultaneous observations of Jovian quasi-periodic radio emissions by the Galileo and Cassini spacecraft, *J. Geophys. Res.*, *109*, A09S07, doi:10.1029/2003JA010263.
Joy, S. P., M. G. Kivelson, R. J. Walker, K. K. Khurana, C. T. Russell, and T. Ogino (2002), Probabilistic models of the Jovian magnetopause and bow shock locations, *J. Geophys. Res.*, *107*, 1309, doi:10.1029/2001JA009146.
Kimura, T., F. Tsuchiya, H. Misawa, A. Morioka, H. Nozawa, and M. Fujimoto (2011), Periodicity analysis of Jovian quasi-periodic radio bursts based on Lomb-Scargle periodograms, *J. Geophys. Res.*, *116*, A03204, doi:10.1029/2010JA016076.
Kimura, T., et al. (2015), Transient internally driven aurora at Jupiter discovered by Hisaki and the Hubble Space Telescope, *Geophys. Res. Lett.*, *42*, 1662–1668, doi:10.1002/2015GL063272.
MacDowall, R. J., M. L. Kaiser, M. D. Desch, W. M. Farrell, R. A. Hess, and R. G. Stone (1993), Quasiperiodic Jovian Radio bursts: Observations from the Ulysses Radio and Plasma Wave Experiment, *Planet. Space Sci.*, *41*, 1059–1072, doi:10.1016/0032-0633(93)90109-F.
Mauk, B. H., J. T. Clarke, D. Grodent, J. H. Waite, C. P. Paranicas, and D. J. Williams (2002), Transient aurora on Jupiter from injections of magnetospheric electrons, *Nature*, *415*, 1003–1005.
McKibben, R. B., J. A. Simpson, and M. Zhang (1993), Impulsive bursts of relativistic electrons discovered during Ulysses' traversal of Jupiter's dusk-side magnetosphere, *Planet. Space Sci.*, *41*, 1041–1058, doi:10.1016/0032-0633(93)90108-E.
Meredith, C. J., S. W. H. Cowley, K. C. Hansen, J. D. Nichols, and T. K. Yeoman (2013), Simultaneous conjugate observations of small-scale structures in Saturn's dayside ultraviolet auroras: Implications for physical origins, *J. Geophys. Res. Space Physics*, *118*, 2244–2266, doi:10.1002/jgra.50270.
Nichols, J. D., J. T. Clarke, J. C. Gérard, D. Grodent, and K. C. Hansen (2009), Variation of different components of Jupiter's auroral emission, *J. Geophys. Res.*, *114*, A06210, doi:10.1029/2009JA014051.
Pryor, W. R., et al. (2005), Cassini UVIS observations of Jupiter's auroral variability, *Icarus*, *178*, 312–326, doi:10.1016/j.icarus.2005.05.021.
Radioti, A., A. T. Tomás, D. Grodent, J.-C. Gérard, J. Gustin, B. Bonfond, N. Krupp, J. Woch, and J. D. Menietti (2009), Equatorward diffuse auroral emissions at Jupiter: Simultaneous HST and Galileo observations, *Geophys. Res. Lett.*, *36*, L07101, doi:10.1029/2009GL037857.
Radioti, A., D. Grodent, J.-C. Gérard, B. Bonfond, J. Gustin, W. Pryor, J. M. Jasinski, and C. S. Arridge (2013), Auroral signatures of multiple magnetopause reconnection at Saturn, *Geophys. Res. Lett.*, *40*, 4498–4502, doi:10.1002/grl.50889.
Vogt, M. F., M. G. Kivelson, K. K. Khurana, R. J. Walker, B. Bonfond, D. Grodent, and A. Radioti (2011), Improved mapping of Jupiter's auroral features to magnetospheric sources, *J. Geophys. Res.*, *116*, A03220, doi:10.1029/2010JA016148.
Vogt, M. F., E. J. Bunce, M. G. Kivelson, K. K. Khurana, R. J. Walker, A. Radioti, B. Bonfond, and D. Grodent (2015), Magnetosphere-ionosphere mapping at jupiter: Quantifying the effects of using different internal field models, *J. Geophys. Res. Space Physics*, doi:10.1002/2014JA020729.
Waite, J. H., et al. (2001), An auroral flare at Jupiter, *Nature*, *410*, 787–789.
Walker, R. J., and C. T. Russell (1985), Flux transfer events at the Jovian magnetopause, *J. Geophys. Res.*, *90*, 7397–7404, doi:10.1029/JA090iA08p07397.